



**HAL**  
open science

# Crystal structure of Glycine max glutathione transferase in complex with glutathione: investigation of the mechanism operating by the tau class glutathione transferases

Irene Axarli, Prathusha Dhavala, Anastassios C. Papageorgiou, Nikolaos E Labrou

## ► To cite this version:

Irene Axarli, Prathusha Dhavala, Anastassios C. Papageorgiou, Nikolaos E Labrou. Crystal structure of Glycine max glutathione transferase in complex with glutathione: investigation of the mechanism operating by the tau class glutathione transferases. *Biochemical Journal*, 2009, 422 (2), pp.247-256. 10.1042/BJ20090224 . hal-00479161

**HAL Id: hal-00479161**

**<https://hal.science/hal-00479161>**

Submitted on 30 Apr 2010

**HAL** is a multi-disciplinary open access archive for the deposit and dissemination of scientific research documents, whether they are published or not. The documents may come from teaching and research institutions in France or abroad, or from public or private research centers.

L'archive ouverte pluridisciplinaire **HAL**, est destinée au dépôt et à la diffusion de documents scientifiques de niveau recherche, publiés ou non, émanant des établissements d'enseignement et de recherche français ou étrangers, des laboratoires publics ou privés.

# Crystal structure of *Glycine max* glutathione transferase in complex with glutathione: investigation of the mechanism operating by the tau class glutathione transferases

by

Irene Axarli<sup>1</sup>, Prathusha Dhavala<sup>2</sup>, Anastassios C. Papageorgiou<sup>2</sup>, Nikolaos E. Labrou<sup>1\*</sup>

<sup>1</sup>Laboratory of Enzyme Technology, Department of Agricultural Biotechnology  
Agricultural University of Athens, 75 Iera Odos Street, GR-11855-Athens, Greece.

<sup>2</sup>Turku Centre for Biotechnology, University of Turku and Åbo Akademi, BioCity, Turku,  
FIN-20521, Finland

\*To whom correspondence should be addressed

Tel.: +30 (210) 5294308

Fax: +30 (210) 5294308

E-mail: lambrou@aua.gr

## **RUNNING TITLE:**

Crystal structure of *Gm*GSTU4-4•GSH complex

## **KEY-WORDS:**

Herbicide detoxification; induced-fit mechanism; kinetic mechanism; tau class GST; X-ray crystal structure.

## **ABBREVIATIONS:**

CDNB, 1-chloro-2,4-dinitrobenzene; GSH, glutathione; GST, glutathione transferase; G-site, GSH binding site; H-site, electrophile binding site; *S*-(*p*-nitrobenzyl)-glutathione, Nb-GSH.

**ABSTRACT**

Cytosolic glutathione transferases (GSTs) are a multifunctional group of enzymes widely distributed in nature and involved in cellular detoxification processes. The three-dimensional structure of *Glycine max* GSTU4-4 (*GmGSTU4-4*) complexed with glutathione (GSH) was determined by the molecular replacement method at 2.7 Å resolution. The bound GSH is located in a region formed by the beginning of  $\alpha$ -helices H1, H2 and H3 in the N-terminal domain of the enzyme. Significant differences in the GSH binding site (G-site) as compared to the structure determined in complex with S-(p-nitrobenzyl)-glutathione (Nb-GSH) were found. These differences were identified in the hydrogen-bonding and electrostatic interaction pattern and, consequently, GSH was found bound in two different conformations. In one subunit, the enzyme forms complex with the ionized form of GSH whereas in the other subunit with the non-ionized form; only the ionized form of GSH may form a productive and catalytically competent complex. Furthermore, a comparison of the GSH-bound structure with the Nb-GSH-bound structure shows a significant movement of the upper part of  $\alpha$ -helix H4 and the C-terminal part. This indicates an intrasubunit modulation between the G-site and the electrophile binding site (H-site), suggesting that the enzyme recognizes the xenobiotic substrates by an induced-fit mechanism. The reorganization of Arg111 and Tyr107 upon xenobiotic substrate binding appears to govern the intrasubunit structural communication between G- and H-site and the binding of GSH. The structural observations were further verified by steady-state kinetic analysis and site-directed mutagenesis studies.

THIS IS NOT THE VERSION OF RECORD - see doi:10.1042/BJ20090224

Accepted Manuscript

## 1. INTRODUCTION

Glutathione transferases (GSTs, EC. 2.5.1.18, formerly known as glutathione S-transferases) are one of nature's most versatile enzymes. They are able to catalyze a wide range of reactions involving the conjugation of GSH ( $\gamma$ Glu-Cys-Gly) to non-polar compounds that contain an electrophilic carbon, nitrogen or sulfur atom (1-5). In this way, GSTs contribute to the metabolism of drugs, pesticides and other xenobiotics. Some products of oxidative stress are also substrates. Hydroperoxides, for example, are formed by the action of active oxygen species that are generated both as normal by-products of aerobic metabolism and as the result of pathogen infection or exposure to certain abiotic agents (3).

GSTs are an ancient and diverse protein family, existing as multigene families in bacteria, fungi, animals and plants (4). Members of different GST classes have similar tertiary and quaternary structures. Each GST subunit consists of two domains: an N-terminal  $\alpha/\beta$  thioredoxin-like fold and a C-terminal all  $\alpha$ -helical structure. The N-terminal domain provides the interactions needed for specific recognition of GSH, forming the G-site. The C-terminal domain harbors the interactions needed to bind the second electrophilic substrate, constituting the H-site (2-4).

Detailed studies of plant GSTs are required because of the considerable agronomic potential of these enzymes with regard to herbicide selectivity, tolerance and environmental safety (6, 7). The plant-specific *phi* and *tau* GST classes are primarily responsible for herbicide detoxification, exhibiting class specificity in substrate preference. Different classes of herbicides such as triazines, thiocarbamates, chloroacetanilides, diphenylethers, aryloxyphenoxypropionates can be metabolized by GSTs (7). Herbicide selectivity and tolerance is based primarily on the differential ability of plant species to detoxify a herbicide, resulting in the formation of a herbicide-GSH conjugate in the resistant but not in the susceptible species (8, 9).

In the present report, the mechanism of GSH binding in a *tau* class GST from *Glycine max* was investigated by X-ray crystallography, kinetic analysis and site-directed mutagenesis. The isoenzyme *GmGSTU4-4* was recently cloned and characterized (10). The enzyme is a homodimer protein, exhibits wide substrate specificity and adopts the canonical GST fold but with a number of functionally important differences in the hydrophobic substrate binding site, the linker segment and the C-terminal region. Comparison of the structure of GSH-bound enzyme (present study) with the Nb-GSH-bound enzyme (10) (Nb-GSH is considered as a product analogue) showed that structural rearrangements occur within selected regions upon GSH binding. These rearrangements are coupled to alterations in the localization of the upper part of  $\alpha$ -helix H4 and the C-terminal. Moreover, the present paper provides the first structure-based evidence for an induced fit mechanism of *tau* class GSTs previously been postulated only for class *pi* and *phi* enzymes (11-12).

## 2. MATERIALS AND METHODS

### 2.1. Materials

Reduced glutathione, 1-chloro-2,4-dinitrobenzene (CDNB), S-(p-nitrobenzyl)-glutathione (Nb-GSH) and all other enzyme substrates were obtained from Sigma-Aldrich, USA. XL1-Blue *E. coli* cells and *Pfu* DNA polymerase were purchased from Stratagene (USA). All other molecular biology reagents were obtained from Promega (UK).

### 2.2. Methods

### 2.2.1. Cloning, expression and purification of *GmGSTU4-4*.

Cloning, expression and purification of *GmGSTU4-4* was carried out as described by Axarli et al. (10).

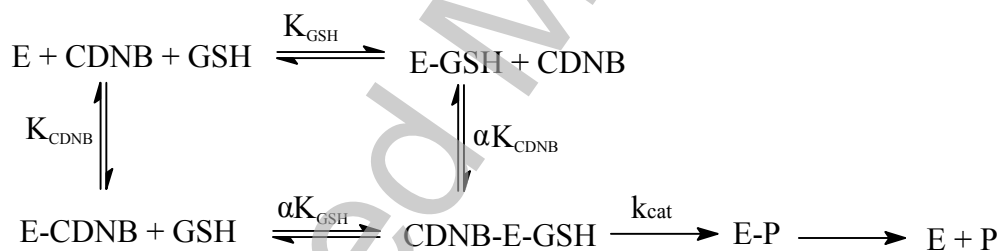
### 2.2.2. Assay of enzyme activity and protein.

Enzyme assays for the CDNB conjugation reactions were performed at 37 °C according to published methods (13-15). Observed reaction velocities were corrected for spontaneous reaction rates when necessary. All initial velocities were determined in triplicate in buffers equilibrated at constant temperature. Turnover numbers were calculated on the basis of one active site per subunit. Protein concentration was determined by Bradford assay using bovine serum albumin (fraction V) as standard.

### 2.2.3. Kinetic Analysis

Steady-state kinetic measurements for the wild-type enzyme were performed at 37 °C in 0.1 M potassium phosphate buffer, pH 6.5 as described by Axarli et al. (10). For the mutant enzymes initial velocities were determined in the presence of 2.5 mM GSH. CDNB was used in the concentration range of 0.015-1.0 mM. Alternatively, CDNB was used at a fixed concentration (1 mM), and GSH concentration was varied in the range of 0.038-1.0 mM. The apparent kinetic parameters  $k_{cat}$  and  $K_m$  were determined by fitting the recorded steady-state data to the Michaelis-Menten equation by nonlinear regression analysis using the GraFit (Erithacus Software Ltd.) computer program.

Kinetic data were fitted to the equation (1) for the rapid equilibrium random sequential bi-bi model (16-19) according to the following scheme:



$$u = V_{max} [GSH][CDNB] / (\alpha K_{GSH} K_{CDNB} + \alpha K_{GSH} [CDNB] + \alpha K_{CDNB} [GSH] + [GSH][CDNB])$$

(equation 1)

where  $\alpha$  is the coupling factor;  $K_{GSH}$  is the dissociation constant of GSH;  $K_{CDNB}$  is the dissociation constant for CDNB.

Inhibition experiments with Nb-GSH-glutathione were performed over in the presence of fixed inhibitor concentrations ranging from 0-0.113mM.

### 2.3. Site-Directed Mutagenesis.

Site-directed mutagenesis was performed as described by Axarli et al., (10). The pairs of oligonucleotide primers used in the PCR reactions were as follows: for the Tyr107Ala mutation, 5'-AAGAAGATAGCTGATCTTGGAAGG-3'; and 5'-CCTTCCAAGATCAGCTATCTTCTT-3' and for the Tyr107Phe mutation, 5'-AAGAAGATATTTGATCTTGGAAGG-3' and

5'-CCTTCCAAGATCAAATATCTTCTT-3'. The mutant enzyme was expressed and purified as described for the wild-type enzyme (10).

#### 2.4. Spectroscopic studies.

Difference spectra of GSH bound to *GmGSTU4-4* were obtained (14,17) with a Perkin Elmer Lambda 16 double-beam double monochromator UV-VIS spectrophotometer equipped with a cuvette holder that was thermostated at 37 °C. In a typical experiment 1 mM GSH (final concentration) was added to *GmGSTU4-4* (approx. 15 µM subunit concentration) in 1 mL of 0.1 M suitable buffer. The amount of thiolate formed at each pH was monitored with the peak-to-trough amplitude between 240 and 300 nm on the basis of an extinction coefficient  $\epsilon_{240\text{nm}}$  of 5,000 M<sup>-1</sup> cm<sup>-1</sup> after subtraction of the spectral contributions of free enzyme and of free GSH.

#### 2.5. Viscosity dependence of kinetic parameters

The effect of viscosity on kinetic parameters was assayed at 37 °C in 0.1 M potassium phosphate buffer, pH 6.5, containing variable glycerol concentrations (0-40% v/v). Viscosity values ( $\eta$ ) at 37 °C were calculated as described in (20).

#### 2.6. Crystallisation

Crystals of the native type *GmGSTU4-4* were grown by the hanging drop vapour diffusion method. 2 µl of the protein solution (12.5 mg/mL in HEPES 10mM, GSH 10 mM, pH 7.0) were mixed with 2µl of the precipitant solution (tri-sodium citrate 1.2-1.3 M in buffer HEPES 0.1 M, pH 7.4) and then equilibrated against 800 µl of the precipitant solution at 16 °C. Crystals appeared within one day and grew to a maximum size of 0.5x0.15x0.15 mm<sup>3</sup> within 3 days.

#### 2.7. Data collection and processing

Data to 2.7 Å resolution were collected from a single crystal on station X13 in EMBL-Hamburg, c/o DESY. Prior to data collection, the crystal was briefly soaked in mother liquor solution containing 20 % v/v glycerol as a cryoprotectant and subsequently flash-cooled in a liquid nitrogen cryostream. A total of 250 images were collected at 0.8088 Å wavelength using a MAR CCD detector with the crystal-to-detector distance at 185 mm and  $\Delta\phi=0.5^\circ$ . Owing to the weak diffraction of the crystal, the exposure time per image was set to approximately 2 minutes in order to record weak reflections. Data processing was carried out using the HKL suite (21).

#### 2.8. Structure determination and refinement

Calculation of the Matthews coefficient (22),  $V_m$ , indicated the presence of two molecules in the asymmetric unit corresponding to a solvent content of approximately 74%. Molecular replacement was performed by PHASER (23) in the CCP4 programme suite (24) using a poly-alanine model derived from the coordinates of *GmGSTU4-4*•Nb-GSH complex (PDB code 2vo4) at 1.75 Å resolution (10). Location of the two molecules resulted in a Z-score of 61.4. Calculation of an initial electron density map showed reasonably good quality that could allow most of the side-chains to be modelled. Refinement was carried out by REFMAC5 (25) in the CCP4 programme suite. Medium non-crystallographic restraints were used in the initial stages of the refinement. The program COOT was employed to manually build the model (26). The progress of the refinement was monitored by excluding 5% of the reflections for the calculation of the  $R_{free}$ . When the  $R_{free}$  reached 25.8%, the co-ordinates were subjected to Translation/Libration/Screw (TLS) refinement. The TLS Motion Determination (TLSMD) server (<http://skuld.bmsc.washington.edu/~tlsmd/>) was used to obtain suitable fragments for

TLS and restrained refinement. This stage proved useful and led to a further drop in the  $R_{free}$  by approximately 2%. Waters were added to the structure using the automatic procedure of ARP/WARP (27). The overall quality of the structure was assessed by PROCHECK (28) and validation tools in COOT (26).

### 2.9. Protein Data Bank accession code

The refined coordinates of the model and the structure factors have been deposited with the Protein Data Bank under the accession code 3FHS.

## 3. RESULTS & DISCUSSION

### 3.1. Structure determination of the *GmGSTU4-4* in complex with GSH and quality of the final model.

The plant-specific tau GSTs are an important class of enzymes since they are primarily responsible for herbicide detoxification (8, 10, 29). To understand the function of tau GSTs as well as to obtain insights into the mechanism of GSH activation and catalysis, X-ray crystallography, kinetic analysis and site-directed mutagenesis of the *GmGSTU4-4* isoenzyme were employed. The structure presented here in conjunction with the structure of the Nb-GSH-enzyme complex (10) allowed us to make direct observations about the changes that occur to the enzyme in the transition from the GSH-bound complex (which represents a snapshot of the enzyme mechanism before the chemical event takes place) to the Nb-GSH-bound form (which represents a snapshot of the enzyme mechanism after the chemical event).

The purified recombinant *GmGSTU4-4* was co-crystallized with GSH via the hanging drop vapor diffusion method and the structure was determined at 2.7 Å resolution. Details of data collection and refinement statistics are shown in Table 1. The crystals diffracted weakly despite their relative good size. The high solvent content as deduced by the calculation of Matthews coefficient ( $V_m=4.86 \text{ \AA}^3/\text{Dalton}$ ) could explain the reason for the weak diffraction of the crystals.

The Ramachandran plot showed that most of the  $\phi$ ,  $\psi$  pairs for non-glycine and non-proline residues fall within the energetically favorable regions. For example, 99.2 % of residues are found in the core and allowed regions. Three residues (Leu139 from subunit A; Thr143 and Ala131 from subunit B) are found in the disallowed region. Pro55 adopts a *cis*-conformation similar to that in the *GmGSTU4-4*•Nb-GSH complex (10).

### 3.2. Overall structure

The overall structure of *GmGSTU4-4* has been described previously (10). Most of the differences between the previously determined structure and the one reported here are described in the following sections. Two *GmGSTU4-4* subunits form a dimer with globular shape. All plant cytosolic glutathione transferases that belong to tau and phi classes are dimeric proteins (4,8,12,14,29). The homodimer assembly of the native enzyme is displayed in Figure 1a. Each *GmGSTU4-4* subunit folds to form two spatially distinct domains: a small N-terminal  $\alpha/\beta$  domain (residues 1 to 77) and a larger C-terminal  $\alpha$ -helical domain (residues 89 to 219). No significant differences were observed in the overall structure of the N-terminal domains (RMSD 0.18 Å). On the other hand, the RMSD between the C-terminal domains of the two structures is 1.45 Å. Two striking differences were observed in the C-terminal domain (Figure 2) concerning the conformation of the upper part of  $\alpha$ -helix H4 (residues 114WTSKGE120;  $C_\alpha$ -atom displacement > 1.6 Å) and the C-terminal (residues 214KKLGIE219;  $C_\alpha$ -atom displacement > 3 Å). These regions are not involved in any

interactions with symmetry-related molecules in the crystal lattice and therefore their differences cannot be attributed to crystal lattice contacts. In agreement with the *GmGSTU4-4*•Nb-GSH complex, the subunit-subunit interface involves three types of interactions: salt bridges, hydrogen bonds and hydrophobic interactions.

### 3.3. Structural features of the G-site.

In each monomer, one molecule of GSH is bound (Figure 1) in a region formed by the beginning of  $\alpha$ -helices H1, H2 and H3 in the N-terminal domain. Comparison of the present structure with that in complex with Nb-GSH (10) revealed significant differences in the G-site. These differences affect the hydrogen-bonding and electrostatic interaction pattern of GSH with the enzyme. Consequently, GSH is bound in a different conformation in each subunit. Its glycine residue is oriented at a different location and occupies part of the H-site where the nitrobenzyl moiety of Nb-GSH is positioned (10) (Figure 2). In the *GmGSTU4-4*•Nb-GSH structure, the glycyl-carboxylate of the ligand is located in a polar environment able to form strong ionic and hydrogen bonds with the  $\epsilon$ -amino group side chain of Lys40 and two water-mediated hydrogen bonds with Lys215 side chain. In subunit A of the present structure the glycyl part of GSH is located in a region characterized by positive electrostatic potential and it is fixed by a hydrogen bond formed with the side chain oxygen of Tyr107 (Figure 1b). In both subunits, the  $\gamma$ -Glu moiety of GSH points downwards to the internal cavity in agreement with the previous *GmGSTU4-4*•Nb-GSH structure.

A striking characteristic of the active site in *GmGSTU4-4* is the central position of Tyr107. In the Nb-GSH complex the hydroxyl group of Tyr107 points towards the aromatic ring of 4-nitrobenzyl moiety, making an on-face hydrogen bond between the hydroxyl group of its side chain and the  $\pi$ -electron cloud of the benzyl group (Figure 2). This interaction stabilizes the aromatic substrates at their productive orientation. However, in the present GSH-bound structure, Tyr107 stabilizes the glycine moiety of GSH by a strong hydrogen bond (distance 2.8 Å). The hydrogen bond of Tyr107 side chain with the Gly carboxylate of GSH suggests that the hydroxyl group of Tyr107 is protonated. This is further supported by the absence of a positively charged group adjacent of Tyr107. Moreover, the lack of movement of the Tyr107 side chain between the two structures supports the proposal that Tyr107 is not becoming ionized during GSH binding. Thus, Tyr107 does not appear to play a role as a general base to abstract a proton from the thiol group of the substrate in the *GmGSTU4-4*•GSH complex.

On the other hand, the glycyl-part of GSH in subunit B adopts different conformation. Indeed, it is positioned away from Tyr107 and towards an unfavored hydrophobic environment formed by Phe10, Pro12, Leu37, Trp163 and Phe208. These differences probably indicate variations in the ionic state of the glycyl-moiety in subunit A (ionized form) and subunit B (non-ionized) form. It is noteworthy to mention that the positively charged Arg38 in subunit B points towards the solvent, whereas in subunit A it points towards the glycyl-carboxylate of GSH. This further supports the different ionization states of Gly carboxylate in subunit A and B.

In subunit A, the Cys residue of GSH points towards  $\alpha$ -helix H2 and away from the catalytic Ser13 (Figures 1b, 2). In this conformation, the -SH group is accessible to the bulk solvent, pointing towards the H-site. Moreover, it is able to form a hydrogen bond with water molecule W219 (2.8 Å) and make weak contacts with the side-chain carbon atoms of Lys53. W219 is further stabilized at this position by a hydrogen bond formed with Lys40. The location of -SH group towards the solvent and the development of a strong hydrogen bond

with W113 indicate that the –SH group in subunit A may be ionized and able to play a role as a nucleophile in the catalytic reaction. Hence, this mode of interaction between enzyme and GSH may lead to a productive and catalytically competent complex. On the other hand, in subunit B, the –SH group of GSH points away from the H-site and towards the protein interior, indicating that probably the –SH group is in its non-ionized form. In this conformation the -SH group does not seem to be able to play a role as a nucleophile in the catalytic reaction and to produce a catalytically competent complex. Consequently, the enzyme is able to form a complex with the ionized form of GSH (productive binding) in one subunit and with the non-ionized form (unproductive binding) of GSH in the other subunit.

The biological significance of the ability of *GmGSTU4-4* to form an unproductive complex with GSH is unclear. One possibility is that unproductive binding may protect the GSH –SH group from oxidation *in vivo*, under oxidative stress conditions where *GmGSTU4-4* is induced (29). Another possibility is that *GmGSTU4-4* may facilitate delivery of the bound GSH to specific receptors (proteins) or cellular compartments by performing a non-catalytic, possibly regulatory function such as glutathionylation (32). Alternatively, this unexpected finding may be the consequence of a multistep mechanism of GSH binding to the enzyme by which the formation of the catalytic competent complex could proceed in two steps. The first step may correspond to the pre-complex (nonionized form of GSH) observed in this work. The second step could correspond to additional rearrangements of the active site as the GSH-enzyme pre-complex transitions to the active form of the enzyme. The existence of such a two-step binding mechanism has also been suggested for human GST P1-1 based on NMR data (33).

### 3.6. Reorganization of the electron-sharing network upon xenobiotic substrate binding.

Recently, the existence of a conserved electron-sharing network that assists the glutamyl  $\gamma$ -carboxylate of GSH to act as a catalytic base accepting the proton from the -SH thiol group of GSH, forming an ionized GSH has been reported (34). The proposed electron-sharing network derives from two critical residues that form ionic bridge interactions between the negatively charged glutamyl carboxylate group of GSH, a positively-charged residue (primarily Arg) and a negatively-charged residue (Glu or Asp) stabilized by hydrogen-bonding networks with surrounding residues (Ser, Thr) and/or water-mediated contacts. This network appears to be a functionally conserved motif that contributes to the “base-assisted deprotonation” model suggested to be essential for the GSH ionization step of the catalytic mechanism. In the *GmGST*-GSH complex, the strictly conserved residues Arg18, Glu66, Ser67 and Asp103 appear to form the proposed electron-sharing network (Figure 3a,b). The motif is stabilized by different interactions in subunit A and B. Interestingly, the network observed in the Nb-GSH complex (Figure 3c) is more alike to that observed in subunit A (productive binding) since the conformation of glutamyl  $\gamma$ -carboxylate group of GSH is similar (Figure 3a,c). In addition, Glu66 interacts through a hydrogen bond with glutamyl  $\alpha$ -carboxylate of GSH (Figure 3b, subunit B), supporting the idea of the non-ionized state of GSH in subunit B, whereas in subunit A and in the Nb-GSH complex (Figure 3c) it forms a hydrogen bond with the  $\alpha$ -amino group of  $\gamma$ -glutamyl moiety, in agreement with the proposal of an ionized state of GSH in subunit A.

Based on Quantum mechanics/Molecular mechanics (QM/MM) calculations it was recently proposed (35) that the GSH activation by GSTs is accomplished by a water-assisted proton-transfer mechanism that takes into account the suggested roles of the GSH  $\gamma$ -glutamyl carboxylate group and the active-center water molecules. According to this mechanism,

following a conformational rearrangement of GSH, a water molecule acting as a bridge is able to transfer the proton from the GSH thiol group to the GSH  $\gamma$ -glutamyl carboxylate group. The two different conformations of bound GSH identified in the present study may represent two snapshots of the conformational rearrangement of GSH in the water-assisted proton-transfer mechanism. Indeed, a putative bridge of a network of water molecules in the region of electron-sharing network does exist (e.g. W25, W38, W154, W219).

### 3.7. Reorganization of H-site upon xenobiotic substrate binding.

An intriguing difference between the structure of the enzyme•Nb-GSH complex and the structure presented here is the movement of the side chain of residue Arg111. In the enzyme•Nb-GSH- structure, the guanidine group of this residue is in hydrogen-bonding distance (2.7 Å) with the hydroxyl group of Tyr107, whereas in the GSH-complexed enzyme, the distance is about 5 Å (Figure 2b). This represents a 2.3 Å movement of the guanidine group away from the position found in the Nb-GSH complexed enzyme. In this context, and taking into account that the GSH-glutamate portion binds to the enzyme in a similar manner in both the Nb-GSH and GSH complexed structures, the mechanism of GSH binding can be described as follows: the GSH-glutamate binds first, followed by the filling of the H-site by the xenobiotic substrate. Then, Arg111 from the topmost region of  $\alpha$ -helix H4 moves towards Tyr107 to make a hydrogen bond with the hydroxyl group of Tyr107. Translocation of Arg111 to its new position and the loss of the hydrogen bond of Tyr107 with the Gly oxygen of GSH may promote reorientation of GSH to its correct position for catalysis. This translocation of GSH is reinforced by the large structural transition observed at the C-terminal part and  $\alpha$ -helix H4. The interactions of the central residues Tyr107 and Arg111 assisted by large conformational changes in the upper part of  $\alpha$ -helix H4 (residues 114WTSKGEE120) and the C-terminal part (residues 214KKLGIE219) contribute to correct positioning of the xenobiotic ligand in H-site, as shown in Figure 2. In the *GmGSTU4-4*•Nb-GSH complex the C-terminal is positioned over the top of the N-terminal domain as a lid and partially blocks the active site. On the contrary, in the present *GmGSTU4-4*•GSH structure the C-terminal adopts a different conformation and folds away from the entrance of the active site. In its new orientation, it is stabilized mainly by the N-aromatic interaction formed between Arg213 and Phe170 of the  $\alpha$ -helix H4 and a hydrogen bond with the carbonyl group of Trp114.

Similar reorganizations have been observed in other GSTs as for example in human GSTA1-1 (hGSTA1-1). The hGSTA1-1 isoenzyme has a flexible C-terminal segment that forms a helix ( $\alpha$ 9) closing the active site upon substrate binding (36,37). Crystal structure analysis of hGSTA1-1 has shown that the apoenzyme, lacking an active-site ligand, is characterized by missing electron density for the 14 amino acid residues closest to the C-terminus. In contrast, hGSTA1-1 in complex with the product analog S-benzylglutathione has a well-formed helix ( $\alpha$ 9) involving residues 210–220.

### 3.8. Kinetic analysis of the GSH conjugation to CDNB with the wild type enzyme.

The differences observed between the *GmGSTU4-4*•GSH and *GmGSTU4-4*•Nb-GSH crystal structures may indicate the existence of intrasubunit structural communication between G- and H-site, and probably an increase in the affinity for GSH in the presence of the xenobiotic substrate. Therefore, in order to gain a deeper insight into the mechanism of the catalytic reaction of *GmGSTU4-4*, a kinetic analysis was carried out using CDNB and GSH as substrates (Figure 4, Table 2).

The kinetic mechanism of *GmGSTU4-4* was determined from initial rate data, product inhibition studies, and fitting of the data to the equations for various kinetic mechanisms (19,

38). When GSH was the variable substrate with several fixed concentrations of CDNB, an intersecting pattern of Lineweaver-Burk plot was obtained. Moreover, a similar intersecting pattern was again obtained with CDNB used as the variable substrate at fixed concentrations of GSH (Figure 4). These data were well-fitted to the simplest rapid equilibrium random sequential bi-bi equation or with the mathematically equivalent steady-state ordered bi-bi model. Other reasonable kinetic models (rapid equilibrium ordered bi-bi and steady-state random sequential mechanism) were less reliable on the basis of high mean-square errors. Product inhibition studies with Nb-GSH allow the discrimination between the two possible mechanisms. Product inhibition studies were performed with Nb-GSH at various concentrations of the first substrate and non-saturating concentrations of the second substrate to distinguish these two mechanisms. Inhibition was mixed-type and competitive towards CDNB ( $K_i$  84.6±4.3  $\mu$ M) and GSH ( $K_i$  15.3±1.1  $\mu$ M), respectively (Figure 4). The replots of inhibition data are diagnostic for the rapid equilibrium model. The secondary plots of inhibition constants ( $K_i$ ) versus GSH or CDNB derived from a set of reciprocal plots at different fixed concentrations of Nb-GSH (10-113  $\mu$ M) (with CDNB as the varied substrate and fixed GSH concentrations and *vice versa*) were linear. Data from the Lineweaver-Burk plots (Figure 4a) provide evidence of the convergence of the lines above the abscissa axis, showing a coupling factor  $\alpha = 0.38 \pm 0.03$  with CDNB (Table 2). This fractional number indicates the existence of intrasubunit structural communication between G- and H-site, and that the affinity for GSH increases in the presence of CDNB about 2.6-times.

Conjugation reactions with GSH have been reported for a vast number of compounds and the kinetic mechanism has been clarified (14, 16, 17, 18, 39, 40). In general, the kinetic mechanism of the GST-catalyzed conjugation reaction is very complex and class dependent. For instance, several catalytic mechanisms, including random, ping-pong, and sequential, have been proposed (14, 16, 17, 18, 39, 40), but random binding order of substrates seems to prevail. The phi class maize GST I-catalyzed conjugation reaction between GSH and CDNB, for example, follows a rapid equilibrium random sequential bi bi kinetic mechanism (14), whereas a steady state sequential rapid bi bi mechanism was proposed for other GSTs (39, 40).

### 3.9. Delineation of the role of Tyr107 by site-directed mutagenesis.

In order to shed light at molecular level on the proposed role of Tyr107 imposed by the crystal structure, site-directed mutagenesis studies were carried out. Tyr107 was mutated to Ala and Phe. The mutants were expressed, purified and their kinetic parameters ( $k_{cat}$  and  $K_m$ ) toward CDNB and GSH were determined by steady-state kinetic analysis (Table 3).

The effect of mutations using CDNB as substrate appears to be significantly different from that seen in the fluorodifen/GSH system (10). The Tyr107Ala mutant enzyme shows a significant decrease in  $K_m$  value towards GSH, whereas in the Tyr107Phe mutant the  $K_m$  value is similar to the wild-type enzyme. On the other hand the  $k_{cat}$  values for both mutants have increased, compared to the wild-type enzyme (Table 3). These findings suggest a negative influence of the hydroxyl group on the catalysis (e.g. higher  $k_{cat}$  values for the mutant enzymes) and a negative contribution of the phenol/benzyl group on the affinity of the enzyme for GSH. Presumably, the lack of the critical hydrogen bond between the Gly carboxylate of GSH and Tyr107 is the basis of improved  $k_{cat}$  in the mutant enzymes. Moreover, the absence of the side-chain of Tyr107 as in the case of the Ala mutant may allow the binding of GSH to the enzyme with its correct conformation (e.g. high affinity state), similar to that observed in the enzyme•Nb-GSH complex (10).

The possible influence of the side chain of Tyr107 on the  $pK_a$  values of kinetically relevant ionizations was also analysed. Direct evidence of the formation of GSH thiolate at the active site and its dependence on pH has been studied by difference spectroscopy (14-17). The difference spectrum of the *Gm*GSTU4-4•GSH binary complex shows an absorption band centered at 240 nm that is diagnostic of a thiolate anion (data not shown). The pH dependence of this spectral perturbation at 240 nm identifies an apparent  $pK_a$  of 6.35 for the bound thiol ionization (Table 2). To check the influence of Tyr107 on GSH thiol ionisation, difference spectroscopy experiments were also carried out for the Tyr107Ala and Tyr107Phe mutants. The results showed similar pH dependence for the wild-type and the mutants (Table 3). Accordingly, the possibility that the increased  $k_{cat}$  for the mutants is due to a changed pH dependence of kinetically important ionizations may be ruled out.

Additional interesting results were obtained from viscosity experiments (Figure 5). The  $k_{cat}$  value for the Tyr107Ala and Tyr107Phe mutant enzymes is significantly increased by an increased viscosity, giving a slope of  $k_{cat}^0/k_{cat}$  of 0.48 and 0.41, respectively (Table 2). On the other hand, the effect of viscosity on  $k_{cat}$  for the wild-type enzyme gives a slope of 0.24. The uncatalysed reaction is fully viscosity-independent (41). It is important to note that glycerol does not induce changes in the enzyme secondary structure as detected by far-uv difference spectroscopy (spectra not shown). Recent studies on the catalytic mechanism of *Gm*GSTU4-4 with the herbicide fluorodifen as co-substrate have shown that the rate-limiting step is a physical event probably involving structural transitions of the ternary complex (10). In the case of the wild-type enzyme the intermediate value of the slope ( $0 < \text{slope} < 1$ ) observed for the CDNB/GSH reaction indicates that the rate-limiting step in the enzyme is not dependent on a diffusional barrier (e.g. product release). Instead, other viscosity-dependent motions or conformational changes of the protein may contribute to the rate-limiting step of the catalytic reaction (29).

Leaving-group substitution experiments were carried out with the wild-type enzyme in order to provide further evidence on the rate-limiting step in the conjugation reaction of *Gm*GSTU4-4 with CDNB. The presence of different halogen in substrate provides a different electronegative leaving group, thus resulting in a different rate of GSH conjugation reaction. Substitution of the chlorine atom by the more electronegative fluorine in the CDNB molecule increases about 50-fold the second order rate constant of the uncatalysed reaction with GSH, suggesting that  $\sigma$ -complex formation is rate limiting (29, 34). Substitution of the chlorine by a different halogen (different electronegativity, e.g. fluorine, bromine) suggests that the catalytic reaction of *Gm*GSTU4-4 is barely sensitive to the nature of the leaving group ( $k_{cat}^{FDNB}/k_{cat}^{CDNB} = 2.7$ ,  $k_{cat}^{BDNB}/k_{cat}^{CDNB} = 1.3$ ), indicating that a non-chemical step may be rate limiting in the enzymatic reaction. It is important to note that in the CDNB/GSH catalytic reaction the value of  $k_{cat}/K_m$  ( $\sim 10^2 \text{ s}^{-1} \text{ M}^{-1}$ ) (Table 3) is well below the value beyond which substrate binding is considered to be rate limiting (e.g.  $10^9 \text{ s}^{-1} \text{ M}^{-1}$ ) (42). In addition, the low  $pK_a$  value of the bound thiolate anion ( $pK_a = 6.35$ ) rules out the ionisation of the thiol group of GSH as a rate-limiting process. Altogether, these results are consistent with the idea that the rate-limiting step of the CDNB/GSH catalytic reaction is a physical event probably involving structural motions or conformational changes of the ternary complex. The Tyr107Ala and the Tyr107Phe mutant enzymes show stronger viscosity dependence of  $k_{cat}$ , compared to the wild-type. This provides an indication that both the hydroxyl group as well as the entire phenol group of Tyr107 contributes significantly to the rate-limiting process.

To analyze further the role of Tyr107 detailed kinetic analysis for the mutant enzymes was carried out and the results are listed in Table 2. The results show that the Tyr107Ala mutant

enzyme exhibits a coupling factor  $\alpha = 0.81 \pm 0.02$ , indicating that in the mutant enzyme the affinity for GSH is increased only by approximately 1.2-fold after CDNB binding. This suggests that the mutant enzyme show restricted intrasubunit communication between the G- and H-site compared to the wild-type enzyme. Similar kinetic behavior was also observed for the Tyr107Phe mutant, indicating that the hydroxyl group of Tyr107 plays important role in the synergistic modulation of G- and H-sites, and in favorable modulation of  $k_{cat}$ .

Despite the very low interclass GST sequence identity, which is less than 20% in the C-terminal domain (where Tyr107 is located), there are remarkable analogies between the tau class *GmGSTU4-4* and the mammalian class isoenzymes. Tyr107 is equivalent to Tyr115 of rat GST M1-1 and to Tyr108 of human GST P1-1 (19,43,44). In these isoenzymes, the interactions of the tyrosine hydroxyl group with H-site residues influence negatively the catalysis. The negative contribution in catalysis of a conserved residue is an unusual finding. However, we must point out that it is observed in an aromatic substitution reaction. Other catalyzed reactions require the assistance of this residue as it is observed for *GmGSTU4-4* with the herbicide fluorodifen (10), for the rat GST M1-1 with phenanthrene 9,10-oxide (43) and for the human GST P1-1 with 7-chloro-4-nitrobenz-2-oxa-1,3-diazole (19). GSTs exhibit a remarkable degree of catalytic diversity with single isoenzymes catalyzing multiple reaction types. The extent and type of participation of individual residues in catalysis are highly dependent on the nature of the transition state and the rate-limiting step for the reaction in question.

### 3.10. Conclusion

In this report, questions concerning the structure and function of a tau class GST from soy were addressed. The above described experiments represent the first investigation about the conformation of the GSH when it binds to a tau class GST and allow a direct comparison with the Nb-GSH structure. In the *GmGSTU4-4*•GSH complex reported here significant differences in hydrogen-bonding and electrostatic interaction pattern were found in the G-site as compared to the structure of the enzyme determined in complex with Nb-GSH. The GSH is bound in two different conformations with different ionic states: ionized and non-ionized. In addition, Tyr107 appears to govern the intrasubunit structural communication between G- and H-site and GSH binding. These findings indicate that Tyr107 has a multifunctional role in *GmGSTU4-4* catalysis. The results presented here suggest that plants have probably gained an evolutionary advantage by utilizing a partially disabled active site in the GST enzymes.

### 3.11. Acknowledgement

This work was partially supported by a grant from AUA (Code No: 020083). I.A. gratefully acknowledges A.S. Onassis Public Benefit Foundation for financial support. ACP thanks the Sigrid Jusélius Foundation, the Centre for International Mobility (CIMO), and the Academy of Finland (Grant No: 121278) for research funding. Access to EMBL Hamburg (c/o DESY) was provided by the European Community (Access to Research Infrastructure Action of the Improving Human Potential Programme to the EMBL Hamburg Outstation, contract number: HPRI-CT-1999-00017).

#### 4. REFERENCES

1. Armstrong, R. N. (1997). Structure, catalytic mechanism, and evolution of the glutathione transferases. *Chem. Res. Toxicol.* 10, 2–18.
2. Mannervik, B. and Danielson, U. H. (1988). Glutathione transferases-structure and catalytic activity. *CRC Crit. Rev. Biochem.* 23, 283–337.
3. Oakley, A. J. (2005). Glutathione transferases: new functions. *Curr. Opin. Struct. Biol.* 15, 716–723.
4. Frova, C. (2006). Glutathione transferases in the genomics era: new insights and perspectives. *Biomol. Eng.* 23, 149-169.
5. Hayes, J. D., Flanagan, J. U. and Jowsey, I. R. (2005). Glutathione transferases. *Annu. Rev. Pharmacol. Toxicol.* 45, 51-88.
6. Edwards, R. and Dixon, D. P. (2005). Plant glutathione transferases. *Methods Enzymol.* 401, 169-186.
7. Edwards, R. and Dixon, D. P. (2000). The role of glutathione transferases in herbicide metabolism, In “*Herbicides and Their Mechanisms of Action*” (A. H. Cobb and R. C. Kirkwood, eds.), Sheffield Academic Press, Sheffield, UK., 38–71.
8. Edwards, R., Dixon, D. P. and Walbot, V. (2000). Plant glutathione S-transferases: enzymes with multiple functions in sickness and in health. *Trends Plant Sci.* 5, 193-198.
9. Jepson, I., Lay, V. J., Holt, D. C., Bright, S. W. J. and Greenland, A. J. (1994). Cloning and characterization of maize herbicide safener-induced cDNAs encoding subunits of glutathione S-transferase isoforms I, II and IV. *Plant Mol. Biol.* 26, 1855–1866.
10. Axarli, I., Dhavala, P., Papageorgiou, A. C. and Labrou, N. E. (2009). Crystallographic and functional characterization of the fluorodifen-inducible glutathione transferase from *Glycine max* reveals an active site topography suited for diphenylether herbicides and a novel L-site. *J. Mol. Biol.* 385, 984-1002
11. Stella, L., Nicotra, M., Ricci, G., Rosato, N. and Di Iorio, E. E. (1999). Molecular dynamics simulations of human glutathione transferase P1-1: analysis of the induced-fit mechanism by GSH binding. *Proteins* 37, 1-9.
12. Neufeind, T., Huber, R., Dasenbrock, H., Prade, L. and Bieseler, B. (1997). Crystal structure of herbicide-detoxifying maize glutathione S-transferase-I in complex with lactoylglutathione: evidence for an induced-fit mechanism. *J. Mol. Biol.* 274, 446-453.
13. Axarli, I. A., Rigden, D. J. and Labrou, N. E. (2004). Characterization of the ligandin site of maize glutathione S-transferase I. *Biochem. J.* 382, 885-893.
14. Labrou, N. E., Mello, L. V. and Clonis, Y. D. (2001). Functional and structural roles of the glutathione-binding residues in maize (*Zea mays*) glutathione S-transferase I. *Biochem. J.* 358, 101-110.

15. Labrou, N. E., Karavangeli, M., Tsaftaris, A. and Clonis, Y. D. (2005). Kinetic and in planta analysis of maize glutathione S-transferase I catalysing the detoxification from chloroacetanilide herbicides. *Planta* 222, 91-97.
16. Caccuri, A. M., Ascenzi, P., Antonini, G., Parker, M. W., Oakley, A. J., Chiessi, E., Nuccetelli, M., Battistoni, A., Bellizia, A. and Ricci, G. (1996). Structural flexibility modulates the activity of human glutathione transferase P1-1. Influence of a poor co-substrate on dynamics and kinetics of human glutathione transferase. *J. Biol. Chem.* 271, 16193-16198.
17. Caccuri, A. M., Antonini, G., Nicotra, M., Battistoni, A., Lo, B. M., Board, P. G., Parker, M. W. and Ricci, G. (1997). Catalytic mechanism and role of hydroxyl residues in the active site of theta class glutathione S-transferases. Investigation of Ser-9 and Tyr-113 in a glutathione S-transferase from the Australian sheep blowfly, *Lucilia cuprina*. *J. Biol. Chem.* 272, 29681-29686.
18. Caccuri, A. M., Lo, B. M., Nuccetelli, M., Nicotra, M., Rossi, P., Antonini, G., Federici, G. and Ricci, G. (1998). Proton release upon glutathione binding to glutathione transferase P1-1: kinetic analysis of a multistep glutathione binding process. *Biochemistry* 37, 3028-3034.
19. Lo Bello, M., Oakley, A. J., Battistoni, A., Mazzetti, A. P., Nuccetelli, M., Mazzarese, G., Rossjohn, J., Parker, M. W. and Ricci, G. (1997). Multifunctional Role of Tyr 108 in the Catalytic Mechanism of Human Glutathione Transferase P1-1. Crystallographic and Kinetic Studies on the Y108F Mutant Enzyme. *Biochemistry* 36, 6207-6217.
20. Wolf, A. V., Brown, M. G., and Prentiss, P. G. (1985). Handbook of Chemistry and Physics (Weast, R. C., Astle, M. J. and Beyer, W. H., eds.), pp D-219-D-269, CRC Press, Inc., Boca Raton, F.L.
21. Otwinowski, Z. and Minor, W. (1997). Processing of X-ray diffraction data collected in oscillation mode. In *Methods in Enzymology*, vol. 276 (eds. J. C. W. Carter and R. M. Sweet), pp. 307-326.
22. Matthews, B.W. (1968). Solvent content of protein crystals. *J. Mol. Biol.* 33, 491-497.
23. McCoy, A. J., Grosse-Kunstleve, R. W., Storoni, L. C. and Read, R. J. (2005). Likelihood-enhanced fast translation functions. *Acta Crystallogr. D Biol. Crystallogr.* 61, 458-464.
24. Potterton, E., Briggs, P., Turkenburg, M. and Dodson, E. (2003). A graphical user interface to the CCP4 program suite. *Acta Crystallogr. D Biol. Crystallogr.* 59, 1131-1137.
25. Murshudov, G. N., Vagin, A. A. and Dodson, E. J. (1997). Refinement of macromolecular structures by the maximum-likelihood method. *Acta Crystallogr. D Biol. Crystallogr.* 53, 240-255.
26. Emsley, P. and Cowtan, K. (2004). Coot: model-building tools for molecular graphics. *Acta Crystallogr. D Biol. Crystallogr.* 60, 2126-2132.
27. Morris, R. J., Perrakis, A. and Lamzin, V. S. (2003). ARP/wARP and automatic

interpretation of protein electron density maps. *Methods Enzymol.* 374, 229-244.

28. Laskowski, R., MacArthur, M. W., Moss, D. S. and Thornton, J. M. (1993). PROCHECK: A program to check the stereochemical quality of protein structures. *J. Appl. Crystallogr.* 26, 283-291.

29. McGonigle, B., Keeler, S. J., Lau, S. M., Koeppe, M. K. and O'Keefe, D. P. (2000). A genomics approach to the comprehensive analysis of the glutathione S-transferase gene family in soybean and maize. *Plant Physiol.* 124, 1105-1120.

30. Hegazy, U. M., Mannervik, B. and Stenberg, G. J. (2004). Functional role of the lock and key motif at the subunit interface of glutathione transferase p1-1. *J. Biol. Chem.* 279, 9586-9596.

31. Vargo, M. A., Nguyen, L. and Colman, R. F. (2004). Subunit interface residues of glutathione S-transferase A1-1 that are important in the monomer-dimer equilibrium. *Biochemistry* 43, 3327-3335.

32. Rouhier, N., Lemaire, S. D. and Jacquot, J. P. (2008). The role of glutathione in photosynthetic organisms: emerging functions for glutaredoxins and glutathionylation. *Annu Rev. Plant Biol.* 59, 143-166.

33. Nicotra, M., Paci, M., Sette, M., Oakley, A. J., Parker, M. W., Lo Bello, M., Caccuri, A. M., Federici, G. and Ricci, G. (1998). Solution structure of glutathione bound to human glutathione transferase P1-1: comparison of NMR measurements with the crystal structure. *Biochemistry* 37, 3020-3027.

34. Winayanuwattikun, P. and Ketterman, A. J. (2005). An electron-sharing network involved in the catalytic mechanism is functionally conserved in different glutathione transferase classes. *J. Biol. Chem.* 280, 31776-31782.

35. Dourado, D. F. A., Fernandes, P. A., Mannervik, B. and Ramos, M. J. (2008). Glutathione transferase: New model for glutathione activation. *Chem. Eur. J.* 14, 9591-9598.

36. Kuhnert, D. C., Sayed, Y., Mosebi, S., Sayed, M., Sewell, T. and Dirr, H. W. (2005). Tertiary Interactions Stabilise the C-terminal Region of Human Glutathione Transferase A1-1: a Crystallographic and Calorimetric Study. *J. Mol. Biol.* 349, 825-838.

37. Sinning, I., Kleywegt, G. J., Cowan, S. W., Reinemer, P., Dirr, H. W., Huber, R., Gilliland, G. L., Armstrong, R. N., Ji, X., Board, P. G., Olin, B., Mannervik, B. and Jones, T. A. (1993). Structure determination and refinement of human alpha class glutathione transferase A1-1, and a comparison with the Mu and Pi class enzymes. *J. Mol. Biol.* 232, 192-212.

38. Segel, I. H. (1975). Enzyme kinetics: behaviour and analysis of rapid equilibrium and steady-state enzyme systems, Wiley, New York.

39. Ivanetich, K. M., Goold, R. D. and Sikakana, C. N. (1990). Explanation of the non-hyperbolic kinetics of the glutathione S-transferases by the simplest steady-state random sequential Bi Bi mechanism. *Biochem. Pharmacol.* 39, 1999-2004.

40. Jakobson, I., Warholm, M. and Mannervik, B. (1979). Multiple inhibition of glutathione S-transferase A from rat liver by glutathione derivatives: kinetic analysis supporting a steady-state random sequential mechanism. *Biochem. J.* 177, 861-868.
41. Micaloni, C., Kong, G. K., Mazzetti, A. P., Nuccetelli, M., Antonini, G., Stella, L., McKinstry, W. J., Polekhina, G., Rossjohn, J., Federici, G., Ricci, G., Parker, M. W. and Lo Bello, M. (2003). Engineering a new C-terminal tail in the H-site of human glutathione transferase P1-1: structural and functional consequences. *J. Mol. Biol.* 325, 111-122.
42. Warner, J. R. and Copley, S. D. (2007). Pre-steady-state kinetic studies of the reductive dehalogenation catalyzed by tetrachlorohydroquinone dehalogenase. *Biochemistry* 46, 13211-13222.
43. Johnson, W. W., Liu, S., Ji, X., Gilliland, G. L. and Armstrong, R. N. (1993). Tyrosine 115 participates both in chemical and physical steps of the catalytic mechanism of a glutathione S-transferase. *J. Biol. Chem.* 268, 11500-11511.
44. Caccuri, A. M., Ascenzi, P., Antonini, G., Parker, M. W., Oakley, A. J., Chiessi, E., Nuccetelli, M., Battistoni, A., Bellizia, A., and Ricci, G. (1996). Structural flexibility modulates the activity of human glutathione transferase P1-1. Influence of a poor co-substrate on dynamics and kinetics of human glutathione transferase. *J. Biol. Chem.* 271, 16193-16198.

**Table 1.** Data collection and refinement statistics.

<b>Data collection</b>	
Space group	$P6_1$
Cell dimensions (Å)	a=b=136.2, c=90.7
Resolution range (Å)	100-2.70 (2.75-2.70)
Number of measured reflections	682889
Unique reflections	26170 (1293)
Completeness (%)	99.9 (100.0)
$R_{\text{merge}}$ (%)	6.8 (56.3)
$I/\sigma(I)$	28.9 (3.5)
Mosaicity (°)	0.50
No of molecules	2
Wilson B-factor (Å <sup>2</sup> )	56.4
<b>Refinement</b>	
Resolution range (Å)	59.0-2.7
Reflections (working/test)	24689/1320
$R_{\text{cryst}}/R_{\text{free}}$ (%)	18.9/24.1
No of protein atoms	3656
No of waters	100
<b>RMS deviation from ideal geometry</b>	
Bond lengths (Å)	0.015
Bond angles (°)	1.90
<b>Ramachandran Plot</b>	
Residues in most favourable regions (%)	91.4

Residues in additional allowed regions (%)	6.8
--	-----

---

---

**Average B factors ( $\text{\AA}^2$ )**

---

Main chain	56.1
Side chain	56.5
Waters	54.7
GSH	59.4

---

Accepted Manuscript

THIS IS NOT THE VERSION OF RECORD - see doi:10.1042/BJ20090224

**Table 2.** Kinetic parameters and dissociation constants for CDNB-GSH conjugation by *GmGSTU4-4*.

Kinetic parameter	Wild-type	Tyr107Ala	Tyr107Phe
$K_{\text{CDNB}}$ (mM)	0.34±0.04	0.14±0.02	0.27±0.02
$K_{\text{GSH}}$ (mM)	0.33±0.04	0.12±0.03	0.24±0.02
$\alpha$	0.38±0.03	0.82±0.02	0.75±0.03
Slope of $k_{\text{cat}}^0/k_{\text{cat}}$ (viscosity effect)	0.24±0.007	0.48±0.02	0.41±0.03
$\text{pK}_a$ (GSH ionization)	6.35±0.1	6.42±0.1	6.45±0.1

Accepted Manuscript

**Table 3.** Steady-state kinetic parameters of wild-type and mutants of *GmGSTU4-4* for the CDNB conjugation reaction. The data for the wild-type enzyme were taken from (10) and included for comparison.

Enzyme	$K_m$ ( $\mu\text{M}$ ) (GSH)	$K_m$ , ( $\mu\text{M}$ ) (CDNB)	$k_{\text{cat}}$ ( $\text{s}^{-1}$ ) (CDNB)	$k_{\text{cat}}/K_m$ ( $\mu\text{M}^{-1}\text{s}^{-1}$ ) (CDNB) ( $\times 10^{-2}$ )
Wild-type	159.1 $\pm$ 18.9	158.2 $\pm$ 31.6	2.48 $\pm$ 0.31	1.6
Tyr107Ala	81.53 $\pm$ 6.68	130.50 $\pm$ 6.38	6.39 $\pm$ 0.16	4.9
Tyr107Phe	179.03 $\pm$ 16.57	164.34 $\pm$ 8.40	5.54 $\pm$ 0.15	3.2

### Figure legends

**Figure 1. The structure of *GmGSTU4-4* in complex with GSH.** (a) Stereo ribbon diagram of the dimeric *GmGSTU4-4* structure. The 2-fold axis relating the dimer subunits is perpendicular to the plane of the page. GSH is shown in a stick representation. (b) Stereo ribbon diagram of subunit A. Stereo ribbon diagram of subunit B (c). The protein is represented as a cartoon. Important amino acid residues are shown in a stick representation and labeled. Water molecules (W219 and W221) are shown as spheres and labeled. (d) Omit  $F_{\text{obs}}-F_{\text{calc}}$  electron density map for the bound GSH in subunit A (left) and subunit B (right). The map was calculated after a round of refinement without the ligand and is contoured at  $2.5\sigma$ . The Figures were produced using PyMol (DeLano Scientific).

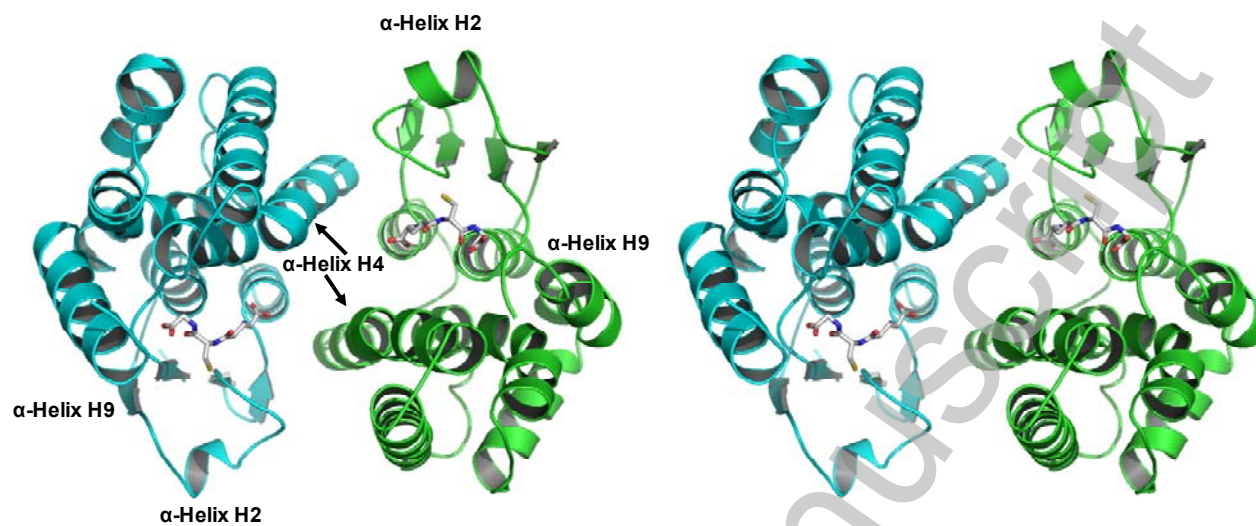
**Figure 2.** Superposition of *GmGSTU4-4* structure in complex with Nb-GSH (light orange) and GSH (light blue). Ligands (Nb-GSH, colored pale green; GSH colored salmon) and selected active site side chains are represented as sticks.  $\alpha$ -Helices H4 and H9 are labelled.

**Figure 3. The electron-sharing network.** Representation of the electron-sharing network of *GmGSTU4-4* in complex with GSH (a, A-subunit; b, B-subunit) and in complex with Nb-GSH (c). In the *GmGSTU4-4*.GSH complex the residues Arg18, Glu66, Ser67 and Asp103 form the proposed electron-sharing network. In the *GmGSTU4-4*.NbGSH complex the residues Ser67, Asp103 and Lys104' (from the neighboring subunit) form the proposed electron-sharing network. The motif appears to be stabilized by a network of hydrogen bonds (dashed lines) involving conserved water molecules (spheres).

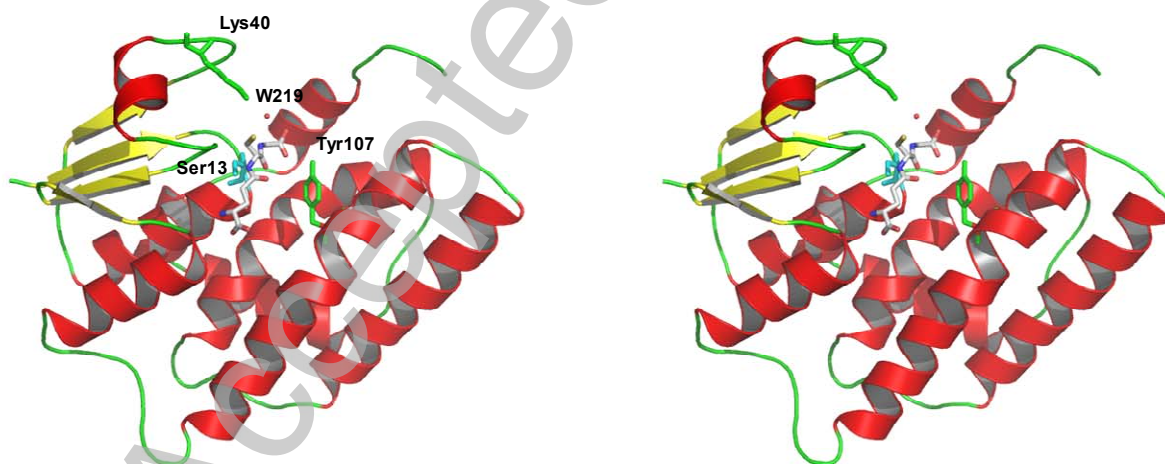
**Figure 4. Kinetic and inhibition analysis of *GmGSTU4-4* in 0.1 M potassium phosphate buffer, pH 6.5.** (a), Initial velocity analysis with GSH as the variable substrate for several fixed concentrations of CDNB (mM): 0.22 ( $\Delta$ ); 0.3 ( $\circ$ ); 0.6 ( $\bullet$ ) and 1 ( $\square$ ). (b), with CDNB as the variable substrate for several fixed concentrations of GSH (mM): 0.5 ( $\Delta$ ); 0.75 ( $\circ$ ); 1.5 ( $\bullet$ ) and 2.5 mM ( $\square$ ). (c) Lineweaver-Burk plots for the determination of inhibition constants for Nb-GSH. Inhibition of *GmGSTU4-4* by Nb-GSH at different GSH concentrations. Enzyme assayed in the absence ( $\circ$ ) or in the presence of Nb-GST: 22.6 ( $\bullet$ ); 45.2 ( $\square$ ); 113.0 mM ( $\blacksquare$ ). (d) Lineweaver-Burk plots for the determination of inhibition constants for Nb-GSH. The enzyme was assayed in the absence ( $\circ$ ) or in the presence of Nb-GST: 22.6 ( $\bullet$ ); 45.2 ( $\blacksquare$ ); 113.0 mM ( $\Delta$ ). (e) Secondary plot of Nb-GSH inhibition on CDNB/GSH conjugation reaction. Secondary plots of  $K_i$  (slope) versus GSH concentration were obtained from a set of reciprocal plots at different fixed concentration of Nb-GSH (with CDNB as the varied substrate and fixed GSH concentrations). (f) Secondary plot of Nb-GSH inhibition on CDNB/GSH conjugation reaction. Secondary plots of  $K_i$  (slope) versus CDNB concentration were obtained from a set of reciprocal plots at different fixed concentrations of Nb-GSH (with GSH as the varied substrate at fixed CDNB concentrations).

**Figure 5. The effect of viscosity on  $k_{\text{cat}}$ .** The effect of viscosity on  $k_{\text{cat}}$  for the CDNB/GSH reaction catalyzed by *GmGSTU4-4* and its Tyr107Ala mutant. Plot of the reciprocal of the relative turnover number ( $k_{\text{cat}}^0/k_{\text{cat}}$ ) as a function of relative viscosity ( $\eta/\eta^0$ ) with glycerol as cosolvent for the wild-type, ( $\circ$ ); and for the Tyr107Ala ( $\bullet$ ) and Tyr107Phe ( $\square$ ) mutant enzymes. Lines were calculated by least-squares regression analysis.

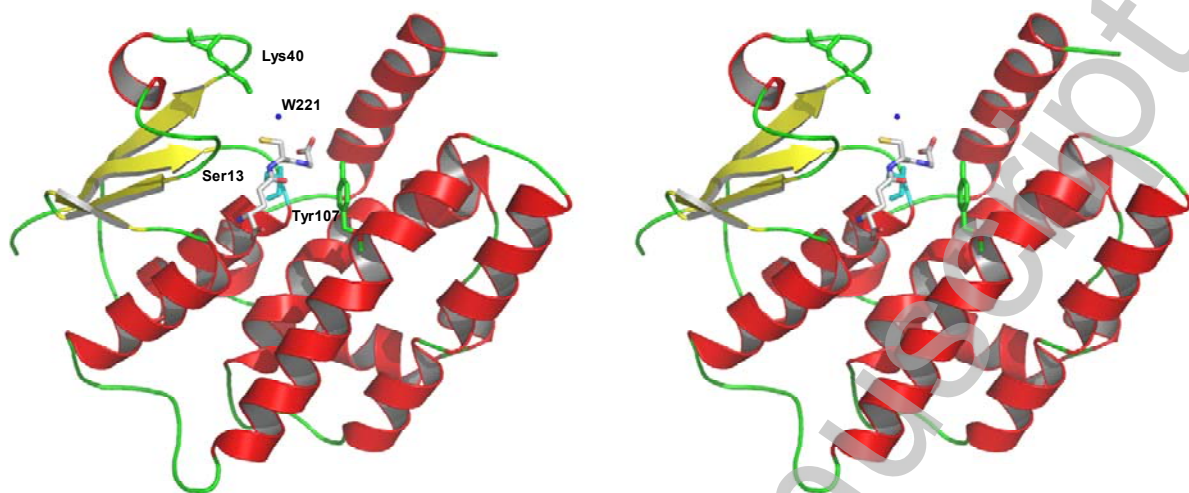
a



b



c



d



Figure 1

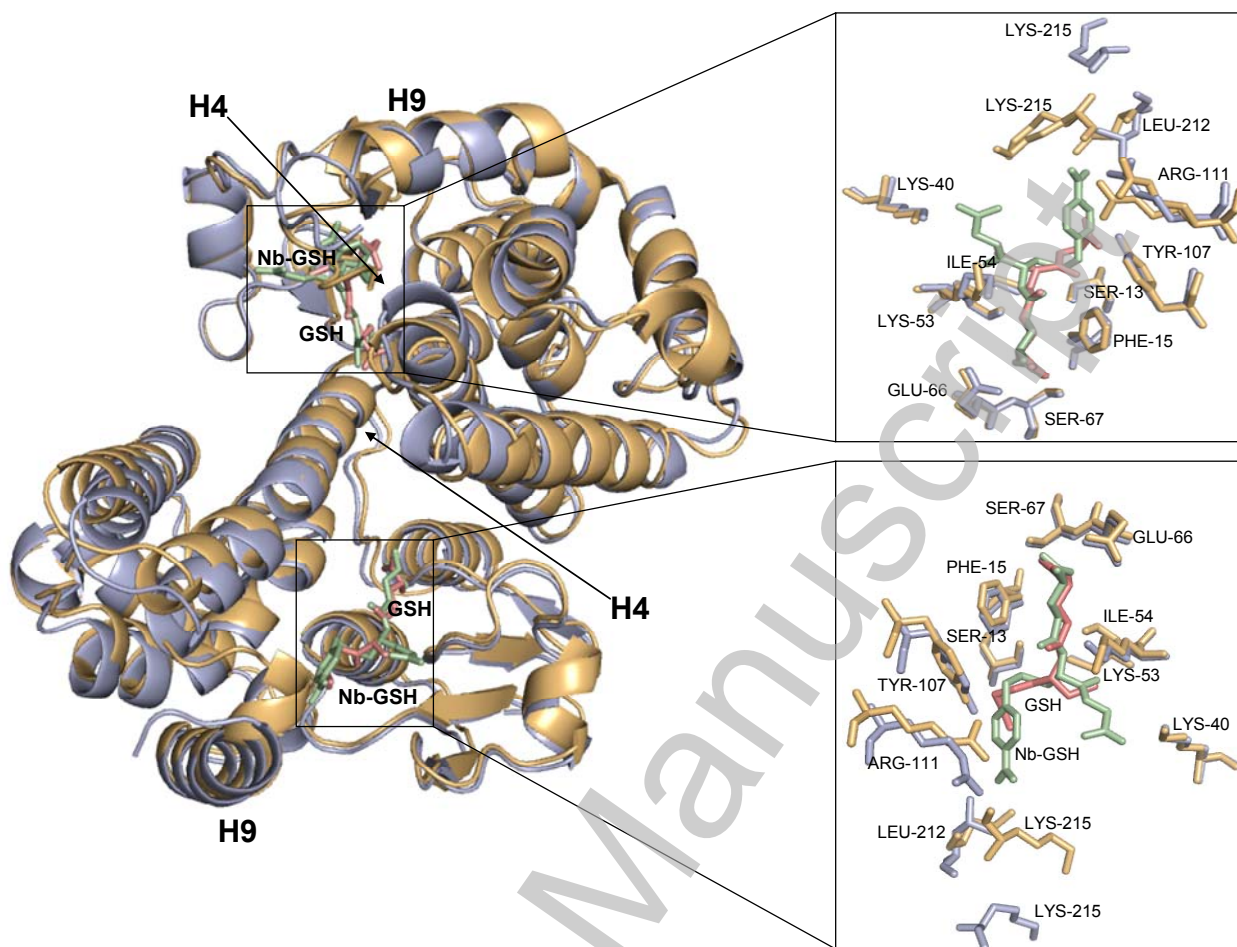


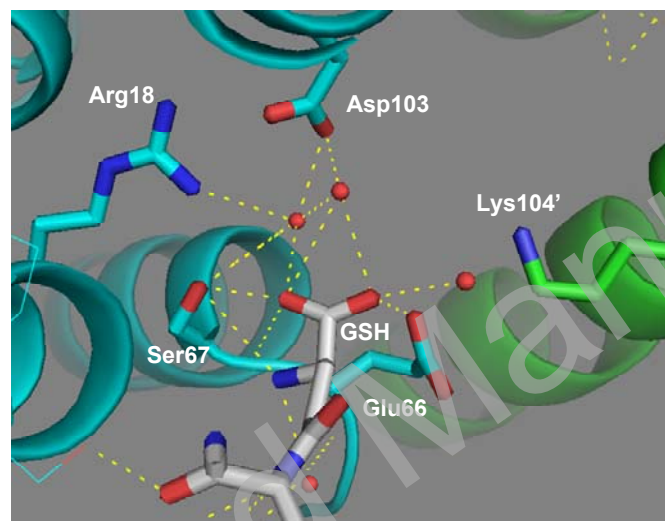
**Figure 2**

THIS IS NOT THE VERSION OF RECORD - see doi:10.1042/BJ20090224

Accepted Manuscript

THIS IS NOT THE VERSION OF RECORD -- see doi:10.1042/BJ20090224

**b**



**c**

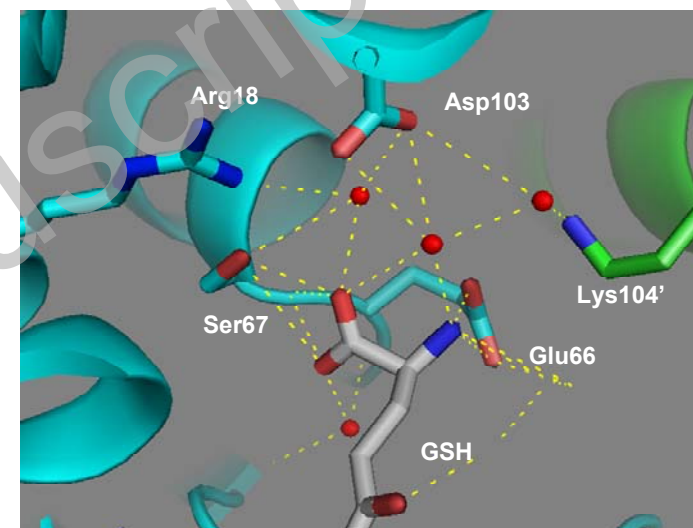


**Figure 3**

Accepted Manuscript

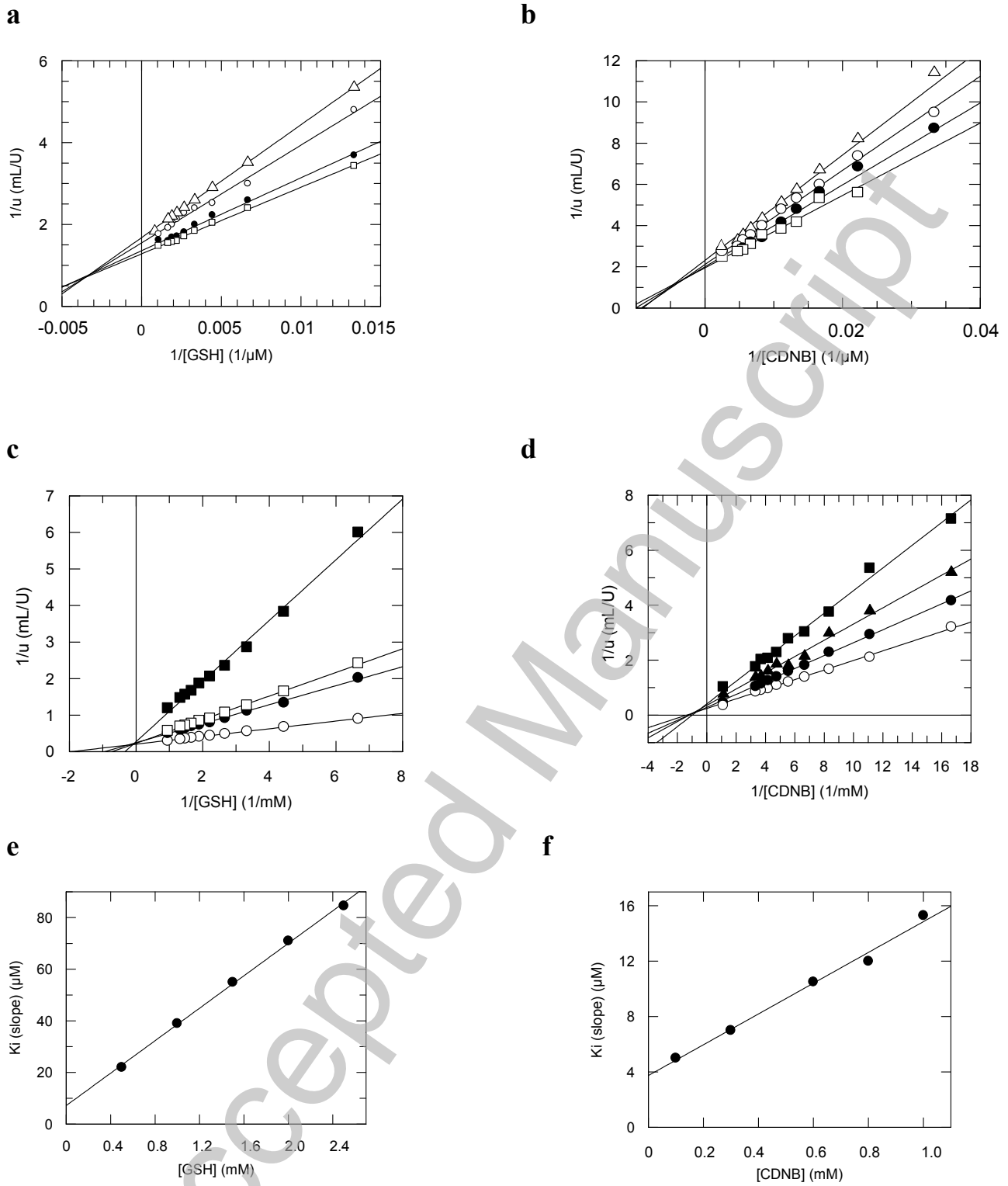


**Figure 4**

THIS IS NOT THE VERSION OF RECORD - see doi:10.1042/BJ20090224

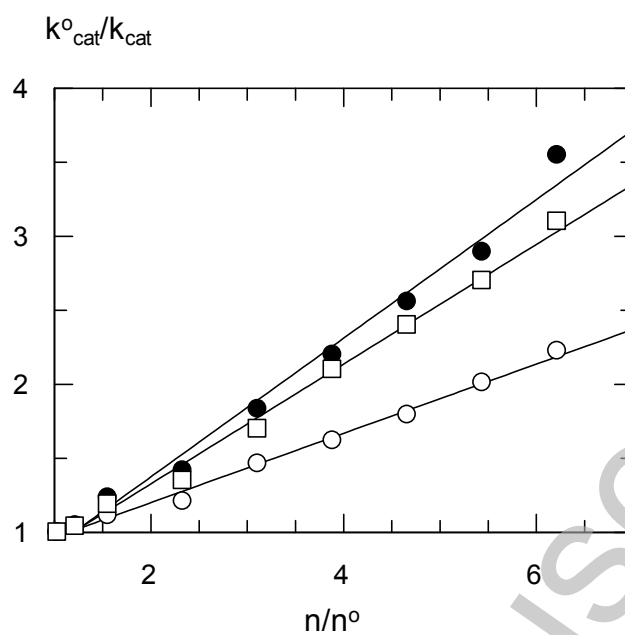


Figure 5